Does tibial sclerosis severity influence bone resorption risk following total knee arthroplasty?

Finite element analysis considering implant design and surgical technique

From Yonsei University, Seoul, South Korea

Cite this article:
Bone Joint Res 2026;15(5):
566–576.

DOI: 10.1302/2046-3758.
155.BJR-2025-0473.R2

Correspondence should be sent to Kyoung-Tak Kang
tagi1024@gmail.com

J. Y. Park,[1] K. K. Park,[2] J-H. Nam,[3,4] M. C. Hwang,[3] K-T. Kang,[3,4] B. W. Cho[5]

[1]Department of Orthopaedic Surgery, Yongin Severance Hospital, Yonsei University College of Medicine, Yongin, South Korea
[2]Department of Orthopaedic Surgery, Severance Hospital, Yonsei University College of Medicine, Seoul, South Korea
[3]Skyve R&D LAB, Skyve Co. LTD., Seoul, South Korea
[4]Department of Mechanical Engineering, Yonsei University, Seoul, South Korea
[5]Department of Orthopaedic Surgery, Gangnam Severance Hospital, Yonsei University College of Medicine, Seoul, South Korea

Aims

Stress shielding, particularly affecting the proximal medial tibial bone, is a significant concern following total knee arthroplasty (TKA). This study investigates how tibial sclerosis severity, implant configurations, and rotational alignment techniques influence bone resorption patterns in the medial proximal tibia.

Methods

Finite element analysis (FEA) was performed using tibial models with four sclerosis levels (0 to 3) representing progressive sclerosis penetration. Four implant configurations combining baseplate shapes (symmetrical vs anatomical) and keel designs (longer (40 mm) vs shorter (30 mm)) were evaluated with two rotational alignment protocols, generating 32 models (4 × 4 × 2). Bone resorption rates in four medial cortical regions were quantified using strain energy density (SED) criteria.

Results

A dose-dependent relationship was demonstrated between sclerosis severity and bone resorption rates. In the total medial cortical region, a substantial increase occurred at Level 3 over Level 0 (67.8% vs. 64.8%, respectively, $p < 0.001$). Keel design emerged as the dominant factor, with shorter keels demonstrating significantly lower absolute resorption rates than longer keels across all sclerosis levels (59.9% to 64.0% vs. 69.8% to 71.7%, $p = 0.029$). However, when changes were analyzed relative to baseline sclerosis severity, shorter keels exhibited significantly greater increases in bone resorption rates than longer keels (4.1% vs 1.9% at Level 3, $p = 0.029$), indicating greater sensitivity to sclerosis progression. Contrary to implant configurations, no significant differences were observed between the maximum-coverage method and Insall's method across all sclerosis severity levels ($p = 0.486$).

Conclusion

Proximal medial tibial sclerosis severity demonstrates a clear dose-dependent relationship with bone resorption risk following TKA. Although shorter keel configurations provide lower absolute bone resorption rates, they exhibit greater sensitivity to sclerosis progression than longer keels. Rotational alignment techniques showed no significant effects on bone resorption patterns in sclerotic bone conditions. These findings support preoperative sclerosis assessment for surgical planning and highlight the complex interaction between implant design and bone quality.

Bone & Joint Research

Article focus

- How does tibial sclerosis severity influence bone resorption risk in the medial proximal tibia following total knee arthroplasty (TKA)?
- What is the impact of different implant configurations (baseplate shapes and keel designs) on bone resorption patterns in sclerotic bone conditions?
- Do rotational alignment techniques (maximum-coverage method vs Insall's method) affect bone resorption in the presence of tibial sclerosis?

Key messages

- Tibial sclerosis severity demonstrates a dose-dependent relationship with bone resorption risk following TKA, with substantial increases at extensive sclerosis levels (Level 3: 67.8% vs Level 0: 64.8%, $p < 0.001$).
- Medialized shorter keel designs achieve lower absolute bone resorption rates than longer keels (59.9% to 64.0% vs. 69.8% to 71.7%), but show greater sensitivity to sclerosis progression (4.1% vs 1.9% increase at Level 3).
- Rotational alignment techniques and tray geometry (symmetrical vs anatomical) have no significant effect on bone resorption patterns in sclerotic bone conditions.

Strengths and limitations

- Systematic evaluation of 32 finite element models combining multiple variables (4 sclerosis levels × 4 implant configurations × 2 alignment techniques).
- Controlled biomechanical analysis isolating the effects of sclerosis severity while controlling for confounding variables.
- Validation against published clinical data showing comparable bone resorption rates.
- Single-patient model limiting generalizability across different anatomies and bone qualities.
- Idealized geometrical sclerosis patterns that do not fully capture complex clinical presentations.
- Focus on immediate postoperative biomechanics without modelling long-term bone remodelling processes.

Introduction

Total knee arthroplasty (TKA) has demonstrated excellent long-term results in treating end-stage knee osteoarthritis.[1] However, stress shielding, particularly affecting the proximal medial tibial bone, remains a significant biomechanical concern.[2-4] Proximal tibial bone loss following TKA underscores the critical importance of implant geometry, thickness, and material properties in mitigating stress-shielding effects.[5-8] Recent evidence indicates that thicker cobalt-chromium tibial baseplates exacerbate stress shielding, while revised designs and titanium components can reduce this effect.[9]

The underlying mechanisms of stress shielding in TKA are multifactorial, involving complex interactions among the implant design, material properties, and surgical techniques.[10-13] Traditional clinical studies investigating stress shielding face limitations due to difficulties controlling confounding variables such as patient activity level, bone mineral density, and surgical variability.[6,14,15] Consequently, those factors can obscure clear relationships between implant characteristics and bone response.

Finite element analysis (FEA) is a valuable method that provides controlled and reproducible conditions for testing biomechanical hypotheses.[2,16,17] Previous FEA using 30 finite element models (FEMs) reported significant differences in stress distribution in the medial proximal tibial bone according to tibial component design.[18] However, that investigation used homogeneous bone models, limiting its ability to fully replicate actual surgical scenarios, in which bone quality varies considerably. Additionally, previous clinical research has suggested that sclerotic bone can contribute to stress shielding development, particularly when the implant's keel overlaps sclerotic areas.[19] That finding suggests that the presence and extent of bone sclerosis might be associated with alterations in the biomechanical environment around tibial implants. Nevertheless, studies explicitly evaluating the relationship between bone sclerosis severity and stress shielding are lacking.

Therefore, we investigated how variations in sclerosis severity, along with diverse implant configurations and rotational alignment techniques, influence bone resorption in the medial proximal tibia area. We hypothesized that increased sclerosis severity would result in greater proximal medial tibial bone resorption, regardless of implant configuration or rotational alignment technique. Additionally, we hypothesized that although medialized shorter keel implants would demonstrate lower bone resorption rates than longer keels, they would show greater sensitivity to increasing sclerosis severity.

Methods

FEM development

Our study protocol was approved by the Institutional Review Board of Yongin Severance Hospital (No. 9-2025-0074). A retrospective study was conducted using high-resolution knee calculated tomography scans (0.6-mm slice thickness, 100 kVp, 150 mAs) from a 65-year-old male patient with osteoarthritis. The images were segmented in Zift (Skyve, South Korea) to generate a 3D tibial model, which was imported into OnKnee-U (Skyve).

Sclerosis modelling

To model medial tibial sclerosis, the medial compartment was partitioned and assigned sclerotic material properties. The location and extent of sclerotic regions were designed to simulate clinically relevant scenarios where tibial sclerosis overlaps with the implant keel, as this condition has been associated with stress shielding development. Sclerosis severity was systematically classified into four distinct levels: Level 0, no sclerosis (control); Level 1, sclerosis extending inward from the cortical bone margin toward the implant central axis, covering a width equal to 1/5 of the distance from the cortical boundary to the implant central axis along the fin midline; Level 2, sclerosis extending inward covering 2/5 of this distance; and Level 3, sclerosis covering 3/5 of the same distance, thus involving partial penetration of the implant fin into the sclerotic region (Figure 1). The sclerotic region extended vertically in the distal direction from the tibial plateau resection surface throughout the entire depth of the region of interest (ROI), representing full-thickness sclerotic bone involvement as can occur in osteoarthritic knees. The cortical bone was modeled with a uniform thickness of 2 mm

Fig. 1
Classification of medial tibial sclerosis severity, modelled as four graded levels of sclerotic involvement progressing from cortical margin to implant fin axis. Level 0 indicates no sclerosis, while Levels 1, 2, and 3 represent sclerosis covering widths of 1/5, 2/5, and 3/5 of the distance from the cortical bone margin toward the implant central axis, respectively.

throughout the proximal tibia, consistent in both circumferential and proximal-distal dimensions.

ROI definition

Specific ROIs were defined on the medial half of the proximal tibial cutting surface, focusing on the axial plane. Within this medial region, a 10 mm wide bone area extending from the medial cortical bone margin was divided into three equal anterior-to-posterior regions of the medial cortical margin: anterior (MCA), middle (MCM), and posterior (MCP), with results also reported for the total (MCT). These four regions were the primary ROIs for bone resorption analysis (Figure 2).

Implant configurations and surgical simulation

Implant configurations were created using the NexGen (Zimmer Biomet, USA) tibial component (size 3) and Persona (Zimmer Biomet) tibial component (size D). Four configurations were evaluated by combining two different baseplate shapes (NexGen: symmetric tray; Persona: anatomical tray) with two different keel designs (NexGen: longer keel; Persona: medialized shorter keel; Figure 3). The medial keel was positioned 0.85 mm medially from the geometrical centre of the tibial baseplate. The evaluated combinations were: symmetrical tray with longer keel (40 mm), anatomical tray with medialized shorter keel (30 mm), symmetrical tray with medialized shorter keel (30 mm), and anatomical tray with longer keel (40 mm). A uniform 2 mm cement layer was inserted between the implant and the resected tibial surface to simulate standard cementing practices. Two rotational alignment protocols were applied to account for surgical variability: Insall's one-third tuberosity to posterior cruciate ligament footprint method and the maximum-coverage method.[20] The rotational position of the tibial component differed by 4.39° between these two protocols. Combining four sclerosis levels, four implant configurations, and two rotational alignment techniques produced 32 implant models and 32 intact counterparts, yielding 64 FEMs total. To quantify stress shielding and bone resorption risk, each implanted model was compared with its corresponding intact (preimplantation) bone model. Each intact model had identical mesh configuration within the ROI and equivalent loading conditions at the tibial plateau contact point, ensuring accurate element-by-element comparison.

FEA setting

The FEA was conducted in Abaqus 6.11 (Dassault Systems, USA). Material properties were assigned based on literature values: cancellous bone (0.4 GPa, 0.3), cortical bone (17 GPa, 0.3), bone cement (2.2 GPa, 0.3), sclerotic bone (1.726 GPa, 0.3), and titanium (110 GPa, 0.3) for elastic modulus and Poisson's ratio, respectively.[21-23] All materials were modeled as homogeneous, isotropic, and linearly elastic. The strain energy density (SED)-based bone resorption analysis used relative strain distribution patterns under physiological loading conditions. A vertical load of 2,030 N was applied, distributed between medial (1,421 N) and lateral (609 N) compartments. This loading scenario employed a 7:3 medial-to-lateral force distribution ratio based on established biomechanical literature.[21,24,25] The anterior-posterior position of the load was determined by the contact point between the femoral component and tibial insert geometry. When implant position changed due to different rotational alignments or designs, the load position was adjusted accordingly to reflect the actual contact mechanics of each configuration. Tie constraints were applied on all interfaces. Mesh convergence was first assessed using the maximum nodal displacement, with a convergence criterion of less than 0.3% change between successive refinements. Furthermore, to ensure the stability of the derived quantities used in the SED-based analysis, convergence of peak Von Mises stress and maximum principal strain within the region of interest was also verified; the relative differences were 0.86% and 1.81%, respectively. Following this multi-criteria validation, an average element size of 0.8 mm was established for all models. All components were meshed using ten-node modified quadratic tetrahedral elements (Abaqus element type: C3D10M).[26] The final models comprised 487,145 elements for cancellous bone, 322,038 elements for cortical bone, 178,222 elements for the tibial baseplate, and 45,661 elements for the cement layer.

Bone resorption calculation

Bone resorption was quantified using a SED criterion.[22] The SED represents the energy stored elastically per unit bone volume and was calculated for each element in both implanted and intact bone models. Elements whose SED in the implanted model were > 75%, lower than the intact model, were classified as resorbed. The resorption rate was calculated

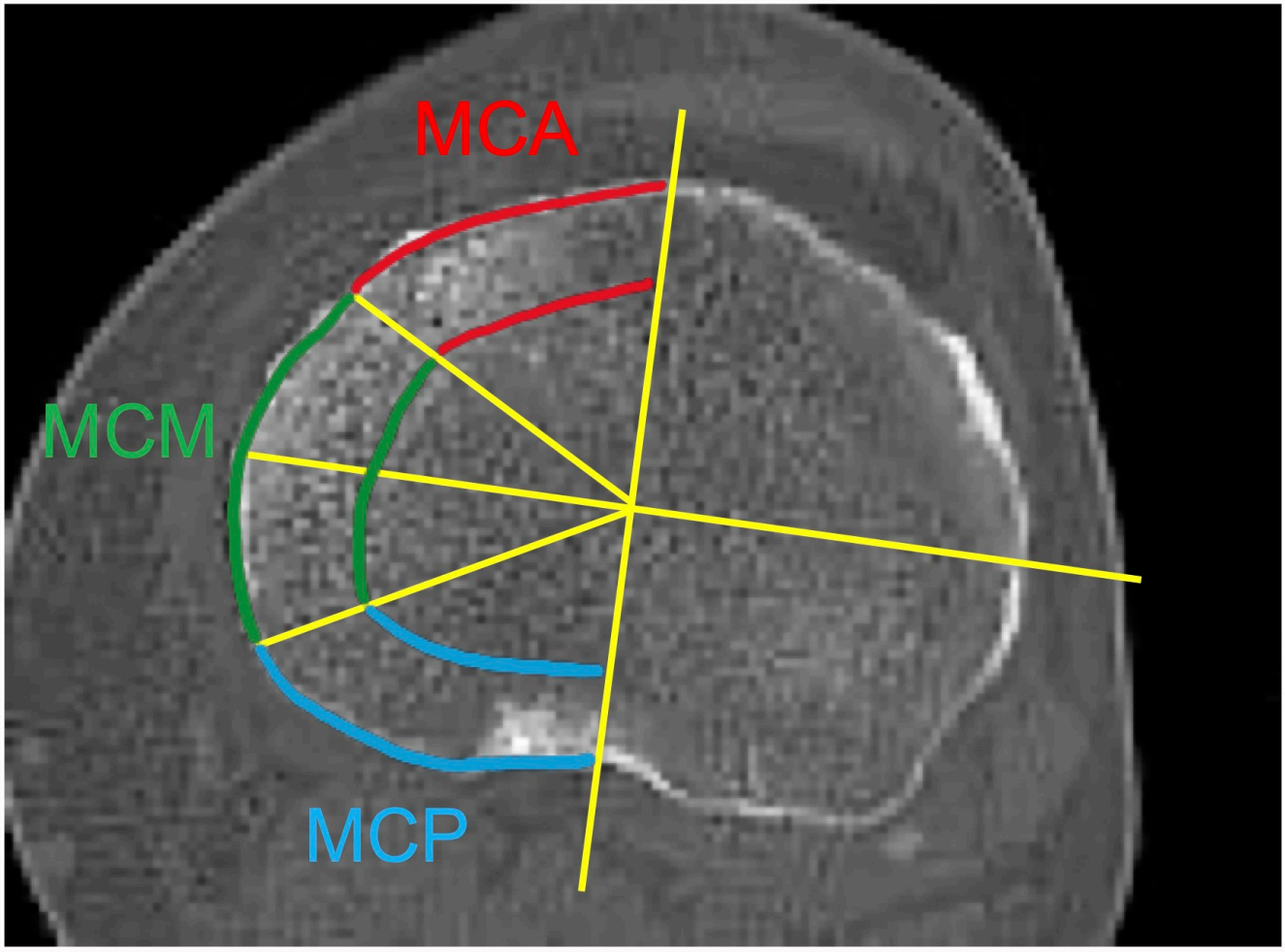

Fig. 2
Definition of regions of interest for bone resorption analysis on the medial cortical margin: anterior (MCA, red zone), middle (MCM, green zone), posterior (MCP, blue zone), and total (MCT, entire medial cortical zone comprising all coloured areas).

as (N_resorbed / N_total) × 100, where N_resorbed is the number of resorbed elements and N_total is the total element count in each ROI.

Outcome measures

The primary outcome was progressive change in bone resorption rates across four sclerosis levels (0 to 3) within each ROI. Secondary outcomes were comparisons of absolute bone resorption rates in the MCT region between: 1) medialized shorter and longer keel configurations; 2) symmetrical and anatomical tray designs; and 3) maximum-coverage and Insall's alignment techniques. Additionally, changes in bone resorption rates relative to baseline across increasing sclerosis levels were evaluated for each subgroup.

FEM validation

To verify FEA accuracy, we compared bone-resorption rates in the proximal 5 mm of tibia with literature values. Park et al[27] documented resorption rates of 53.0% to 61.6%, while our model showed 56.5% to 74.2%. Our lower bound aligned with their range, though our upper bound exceeded their maximum, likely due to differences in patient anatomy and implant design. Overall trends were comparable, supporting model validity.

Statistical analysis

Bone resorption rates are presented as percentages with mean values and ranges across all study variable combinations. Subgroup comparisons between implant configurations at each sclerosis severity level used Mann-Whitney U tests, while comparisons across sclerosis levels within each region used Wilcoxon signed-rank tests. Statistical significance was set at $p < 0.05$. All statistical analyses were performed using R software, v.4.5.0 (R Foundation of Statistical Computing, Austria).

Results

Sclerosis-dependent bone resorption patterns in each ROI

The MCT region showed minimal variation across Levels 1 to 2 (65.1% to 65.4%, Level 1: $p = 0.094$ Level 2: $p = 0.055$ vs Level 0, Wilcoxon signed-rank test) but substantially increased at Level 3 (67.8% (59.7% to 74.2%), $p = 0.008$ vs Level 0), representing a 4.6% relative increase (Table I, Figure 4). The MCA region remained stable at lower sclerosis levels (7.1% to 7.4%,Level 1: $p = 0.672$; Level 2: $p = 0.195$ vs Level 0, Wilcoxon signed-rank test) but markedly increased at Level 3 (8.9% (5.6% to 12.6%), $p = 0.008$ vs Level 0), showing a 23.6% relative increase (Table II). The MCM region demonstrated progressive moderate increases from Level 0 (90.5%) through Level 3

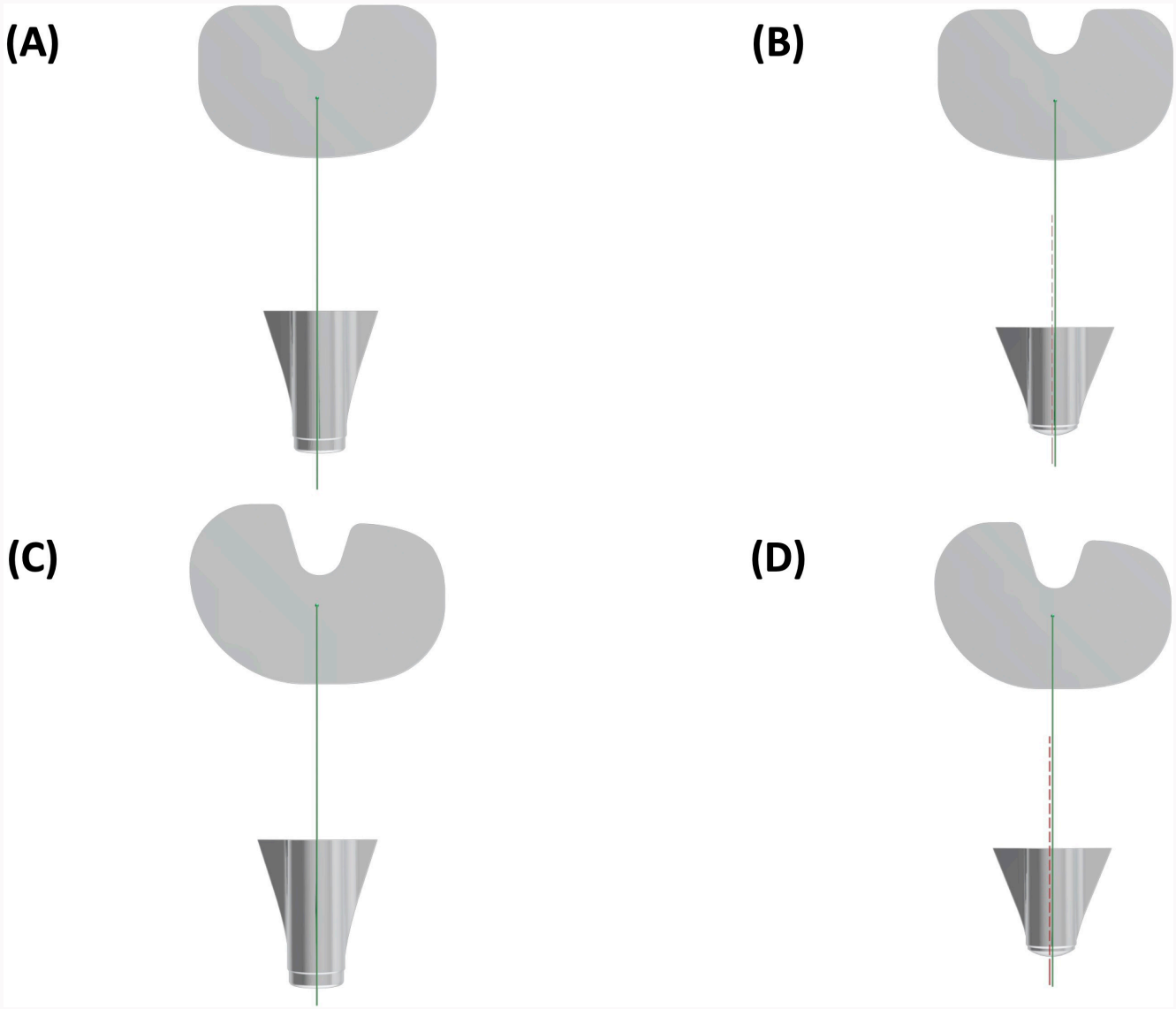

Fig. 3
Schematic illustration of the four implant configurations combining two baseplate shapes (symmetrical vs anatomical) and two keel designs (long vs medialized short). a) Symmetrical tray with longer keel, b) symmetrical tray with medialized shorter keel, c) anatomical tray with longer keel, and d) anatomical tray with medialized shorter keel. The medialized shorter keel is positioned 0.85 mm medially from the geometrical centre of the tibial baseplate (indicated by the green line).

(93.6%, p = 0.008, Wilcoxon signed-rank test), corresponding to a 3.4% relative increase (Table III). The MCP region showed the most pronounced sclerosis effect, progressing from Level 0 (90.1%) through Level 2 (91.4%, p = 0.016, Wilcoxon signed-rank test) to Level 3 (95.5%, p = 0.008, Wilcoxon signed-rank test), reflecting a 6.0% relative increase (Table IV).

Implant configuration comparisons in MCT bone resorption

In the MCT region subgroup analysis, the medialized shorter keel (30 mm) configuration consistently demonstrated significantly lower absolute bone resorption rates than the longer keel (40 mm) design across all levels (59.9% to 64.0% vs 69.8% to 71.7%, p = 0.029, Mann-Whitney U test) (Figure 5). In contrast, symmetrical and anatomical tray designs showed no significant differences across levels (63.9% to 66.6% vs 65.8% to 69.1%, p = 0.686, Mann-Whitney U test), though anatomical trays tended toward higher resorption rates.

When analyzing changes relative to baseline, the medialized shorter keel group demonstrated significantly greater increases in bone resorption rates than the longer keel group across all levels (0.4% to 4.1% vs 0.0% to 1.9%, Level 1: p = 0.029; Level 2: p = 0.029; Level 3: p = 0.029, Mann-Whitney U test) (Figure 5). In contrast, tray designs showed no significant differences in resorption rate changes across any sclerosis level (0.1% to 2.7% vs 0.3% to 3.3%, Level 1: p = 0.885; Level 2: p = 0.686; Level 3 p = 1.000, Mann-Whitney U test).

Surgical technique comparisons in MCT bone resorption

In the MCT region, bone resorption rates showed no significant differences between the maximum-coverage method and Insall's method across all sclerosis levels (63.2% to 65.9% vs 66.5% to 69.8%, p = 0.486, Mann-Whitney U test). Similarly, no significant differences were observed in resorption rate changes relative to baseline between the two techniques

Table I. Bone resorption rates (%) in the medial cortical margin–total region according to the sclerosis severity level, implant configuration, and rotational alignment surgical technique, with Δ (level 3 – level 0) values.

Implant configuration	Rotational alignment surgical technique	Sclerosis severity				
		Level 0	Level 1	Level 2	Level 3	Δ (Level 3 – Level 0)
Symmetrical tray with medialized shorter keel	Maximum-coverage method	56.5	56.9	57.0	59.7	+ 3.2
	Insall's method	59.9	60.0	60.4	63.2	+ 3.4
Anatomical tray with medialized shorter keel	Maximum-coverage method	60.6	61.0	61.7	64.5	+ 3.9
	Insall's method	62.8	63.6	65.3	68.7	+ 5.9
Symmetrical tray with longer keel	Maximum-coverage method	68.3	68.3	68.5	70.2	+ 1.9
	Insall's method	70.9	70.9	70.9	73.1	+ 2.2
Anatomical tray with longer keel	Maximum-coverage method	67.4	67.4	67.5	69.1	+ 1.7
	Insall's method	72.4	72.4	72.4	74.2	+ 1.8

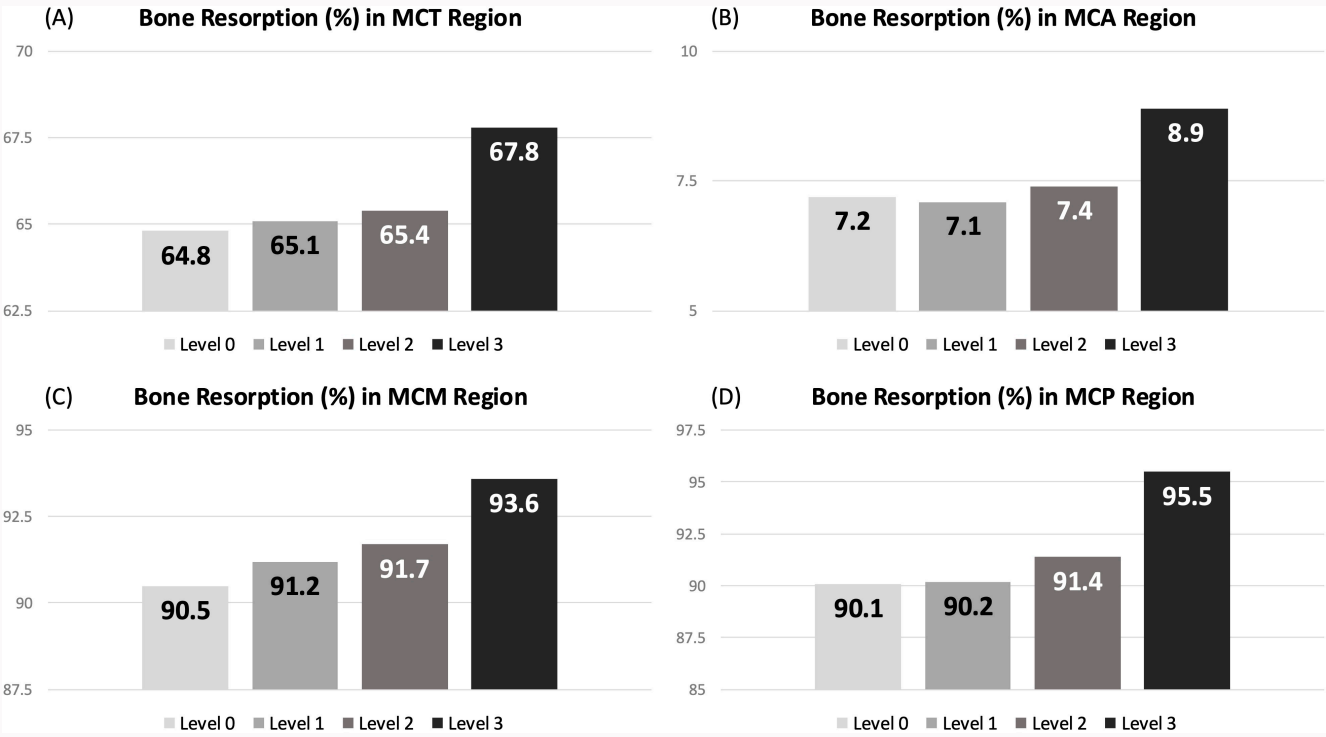

Fig. 4
Bone resorption according to sclerosis severity in four medial cortical margin regions. a) Medial cortical margin–total (MCT) region showing increased bone resorption with higher sclerosis levels. b) Medial cortical margin–anterior (MCA) region with stable resorption at lower levels and sharp increase at Level 3. c) Medial cortical margin–middle (MCM) region with steady increase across all sclerosis levels. d) Medial cortical margin–posterior (MCP) region showing increased bone resorption from Level 0 to Level 3.

(0.2% to 2.7% vs 0.2% to 3.3%, Level 1: p = 0.772; Level 2: p = 0.886; Level 3: p = 0.686).

Discussion

Our FEA demonstrated that as the extent of sclerosis in the proximal tibial medial area increased, bone resorption rates also increased progressively in the medial area beneath the tibial baseplate. This systematic and dose-dependent relationship was observed consistently across all medial cortical regions, and regardless of the implant configuration and rotational alignment surgical technique. Additionally, the medialized shorter keel groups showed statistically significantly lower absolute bone resorption than the longer keel groups, but they demonstrated greater sensitivity to sclerosis progression. Tray geometry, on the other hand, had no significant effect on resorption rates or progression patterns. Furthermore, no significant differences in bone resorption rates or progression patterns were observed between the maximum-coverage method and Insall's method. These results suggest that a preoperative assessment of proximal medial tibial sclerosis severity could facilitate surgical planning strategies to reduce postoperative stress shielding in TKA.

Table II. Bone resorption rates (%) in the medial cortical margin–anterior region according to the sclerosis severity level, implant configuration, and rotational alignment surgical technique.

Implant configuration	Rotational alignment surgical technique	Sclerosis severity			
		Level 0	Level 1	Level 2	Level 3
Symmetrical tray with medialized shorter keel	Maximum-coverage method	6.3	6.1	6.5	8.5
	Insall's method	3.5	3.6	3.8	5.6
Anatomical tray with medialized shorter keel	Maximum-coverage method	7.5	7.5	8.6	10.2
	Insall's method	4.0	4.1	4.2	7.0
Symmetrical tray with longer keel	Maximum-coverage method	8.7	8.7	8.9	9.8
	Insall's method	6.2	6.2	6.7	7.2
Anatomical tray with longer keel	Maximum-coverage method	11.7	11.7	11.2	12.6
	Insall's method	9.4	9.4	9.2	10.5

Table III. Bone resorption rates (%) in the medial cortical margin–middle region according to the sclerosis severity level, implant configuration, and rotational alignment surgical technique.

Implant configuration	Rotational alignment surgical technique	Sclerosis severity			
		Level 0	Level 1	Level 2	Level 3
Symmetrical tray with medialized shorter keel	Maximum-coverage method	86.2	87.3	86.6	89.6
	Insall's method	84.4	84.8	85.7	89.1
Anatomical tray with medialized shorter keel	Maximum-coverage method	89.6	91.0	91.3	92.8
	Insall's method	82.1	85.1	87.6	90.5
Symmetrical tray with longer keel	Maximum-coverage method	92.6	92.6	92.9	94.6
	Insall's method	91.3	91.4	91.2	92.9
Anatomical tray with longer keel	Maximum-coverage method	99.2	99.2	99.2	99.7
	Insall's method	98.4	98.5	98.9	99.5

The biomechanical explanation for these findings lies in the fundamental material properties of sclerotic bone. Sclerotic bone develops through increased osteoblastic activity and reduced bone remodelling, resulting in higher bone density.[28–30] In FEMs, the elastic modulus of sclerotic bone is typically assigned a value of 1.726 GPa, which is higher than the 0.4 GPa of cancellous bone, reflecting its increased stiffness and mechanical strength.[22] These high-stiffness regions preferentially attract mechanical loads, and as the extent of sclerosis increases, they become more dominant in creating load bypass of normal cortical bone structures.[31] This phenomenon parallels biomechanical phenomena widely recognized in joint arthroplasty.[4,31–33] Just as cobalt-chromium tibial components demonstrate greater stress shielding than titanium components due to their higher elastic modulus, and thicker cobalt-chromium baseplates further exacerbate stress shielding effects, the increased stiffness of sclerotic bone creates preferential load pathways that divert stress away from surrounding normal bone tissue.[4,32,34–36] This finding is further supported by observations in total hip arthroplasty, where extensively coated femoral stems demonstrate more pronounced stress shielding effects through similar stiffness-mediated load redistribution mechanisms.[33,37] Consequently, sclerotic bone, with its characteristically increased bone density and higher elastic modulus, establishes preferential load paths that bypass normal cortical bone stimulation, ultimately leading to peripheral bone resorption.

A subgroup analysis focusing on the MCT region revealed significantly lower bone resorption rates with medialized shorter keel configurations than with longer keel designs. When all 32 combinations of implant configuration, sclerosis severity, and surgical technique were ranked by bone resorption rates, the medialized shorter keel configurations showed overwhelming superiority, with 15 of the top 16 combinations using this design and demonstrating significantly lower average resorption rates (61.4% vs 70.2%, $p < 0.001$) (Supplementary Table i). However, in contrast to those keel configuration differences, our results indicate no significant differences between symmetrical and anatomical trays in bone resorption rates in the context of sclerotic bone. This finding is consistent with the FEA study of Cho et al,[18] which compared symmetric tibial components (STC, NexGen) with longer keels versus anatomical tibial components (ATC,

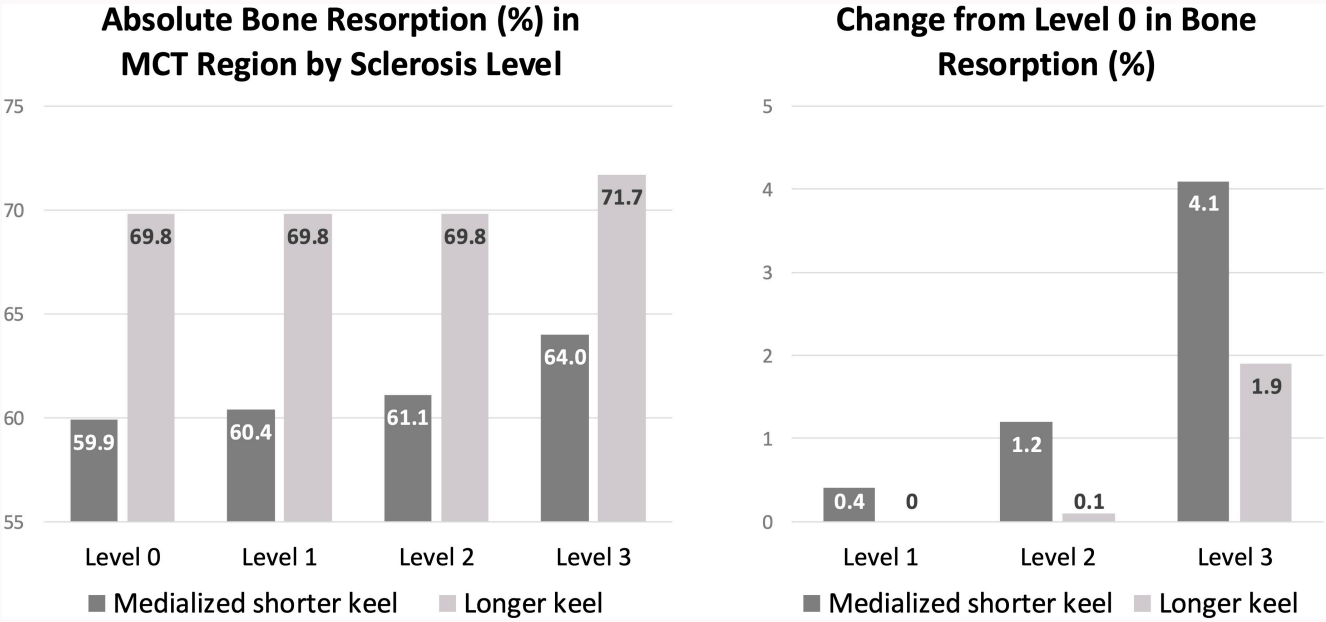

Fig. 5
Comparison of absolute bone resorption and relative increases from baseline between medialized shorter and longer keel designs in the medial cortical margin–total region (MCT).

Table IV. Bone resorption rates (%) in the medial cortical margin–posterior region according to the sclerosis severity level, implant configuration, and rotational alignment surgical technique.

Implant configuration	Rotational alignment surgical technique	Sclerosis severity			
		Level 0	Level 1	Level 2	Level 3
Symmetrical tray with medialized shorter keel	Maximum-coverage method	91.4	90.6	92.3	95.0
	Insall's method	88.8	89.1	92.0	97.2
Anatomical tray with medialized shorter keel	Maximum-coverage method	75.2	75.8	76.6	86.6
	Insall's method	79.7	80.3	83.5	90.4
Symmetrical tray with longer keel	Maximum-coverage method	99.1	99.1	99.1	99.8
	Insall's method	99.0	99.0	99.2	100.0
Anatomical tray with longer keel	Maximum-coverage method	92.4	92.3	92.4	96.3
	Insall's method	95.7	95.7	96.1	98.5

Persona) with medialized shorter keels while controlling for other variables. Their study demonstrated that ATC provided a more favourable stress distribution in the medial proximal tibial bone than STC, and thus better prevented stress shielding. This supports our findings that shorter keel configurations result in lower bone resorption rates. Furthermore, these observed differences are predominantly driven by keel design rather than tray geometry, demonstrating that keel configuration is the more influential factor in bone resorption reduction across all sclerosis severity levels.

Although we confirmed the advantage of medialized shorter keel designs in achieving lower absolute bone resorption rates, our analysis of resorption rate changes relative to increasing sclerosis severity revealed a contrasting pattern. The medialized shorter keel groups demonstrated significantly greater increases in bone resorption rates than the longer keel groups as sclerosis severity progressed. This progressive pattern indicates that although shorter keels show lower absolute resorption rates, they exhibit markedly greater sensitivity to increasing sclerosis severity. This finding also aligns with the study by Cho et al,[19] which demonstrated that when stress concentration occurs due to the stem tip approaching the cortex, ATC showed less stress distribution than STC at the medial proximal tibial bone cutting plane. In our study, the presence of sclerotic bone appears to create stress concentration when the implant approaches or penetrates through it, similar to the stem tip approaching the cortex in the previous study, resulting in an overall increase in bone resorption rates. Consistent with the previous research, ATC configurations showed the greatest changes in resorption rates as sclerosis levels increased. These findings provide

mechanistic insights into the clinical effects of sclerotic bone observed in the previous study of real-world clinical data.[19]

Clinical studies have demonstrated varying outcomes between the maximum-coverage method and Insall's method for tibial component positioning, with one report suggesting improved implant survival and reduced radiolucent line formation with the maximum coverage techniques.[38] The maximum-coverage method was theoretically expected to achieve better outcomes by optimizing load distribution across the tibial plateau and maximizing the contact area between the implant and bone, which should create more uniform stress distribution patterns and prevent excessive load concentration in sclerotic regions. However, contrary to those theoretical expectations, our biomechanical analysis revealed no significant differences in bone resorption rates between the two surgical techniques across all sclerosis severity levels. This finding suggests that in the context of sclerotic bone conditions, the rotational alignment technique might have a less pronounced effect on bone resorption patterns than previously anticipated.

Several limitations of this study should be acknowledged. First, we limited our analysis to a single individual because generating multiple subject-specific FEMs would require prohibitive time and computational resources. This methodology enabled us to assess the influence of tibial sclerosis severity on postoperative bone resorption risk following TKA, while controlling for variables such as body weight, stature, bone morphology, ligament properties, and implant dimensions. However, this single-patient model approach could limit generalizability across different patient anatomies and bone quality variations. The loading conditions simulated normal weightbearing scenarios but did not account for dynamic loading patterns, varying activity levels, or the complex multiaxial forces encountered during daily activities. The sclerosis modelling represents idealized geometrical patterns that do not fully capture the complex, irregular clinical patterns of bone sclerosis observed in actual patients. Furthermore, the granularity of sclerosis segmentation could potentially influence the observed biomechanical trends. While our four-level classification provided a balanced approach to evaluate dose-response relationships, more refined segmentation might reveal non-linear patterns or specific clinical thresholds, whereas coarser segmentation may fail to capture the progressive nature of stress shielding. Additionally, this study focused on immediate postoperative biomechanics without modelling long-term bone remodelling processes or adaptive responses that occur over time. Second, the limitations inherent in all computational simulation studies prevented us from developing clinically applicable tools, such as nomograms for risk factor prediction based on sclerosis severity groupings. Prospective clinical studies incorporating quantitative preoperative sclerosis assessment, standardized surgical techniques, and standardized long-term follow-up are needed to validate these biomechanical predictions and establish evidence-based guidelines for clinical practice. Third, the FEA validation was based on comparison with Park et al,[27] which remains the primary study quantitatively correlating SED-based predictions with clinical bone resorption rates in TKA. Additional validation studies across diverse implant systems would further strengthen the generalizability of this methodology. Lastly, future work will extend this analysis to multiple patient-specific models with heterogeneous anatomy and sclerosis patterns and incorporate time-dependent bone remodelling algorithms under realistic loading conditions. Additionally, prospective clinical studies correlating preoperative sclerosis quantification with postoperative outcomes are planned to validate these predictions. Moreover, future research should investigate the impact of different segmentation approaches to determine the optimal level of resolution required to accurately predict bone resorption risk. This methodological framework could also be applied to systematically evaluate emerging implant designs under various clinical scenarios.

This FEA established that sclerosis severity in the proximal tibia medial area directly correlates with bone resorption risk following TKA, demonstrating systematic dose-dependent increases with a critical threshold at extensive sclerosis. The biomechanical mechanism likely involves sclerotic bone's increased elastic modulus, which may create preferential load pathways that shield normal bone tissue. Regarding implant configuration, the medialized shorter keel demonstrated reduced absolute bone resorption compared with longer keel designs, but exhibited greater sensitivity to sclerosis progression. No significant differences were observed between symmetrical and anatomical trays or between rotational alignment methods. Future research should focus on correlating these finite element predictions with actual clinical outcomes, including implant survival and radiological evidence of bone remodelling over extended follow-up periods.

Supplementary material

Table presenting the complete ranking of bone resorption rates across all 32 combinations of implant configuration, sclerosis severity, and rotational alignment technique in the medial cortical margin–total region.

References

1. **Lee CR**, **Park DH**, **Heo KS**, **Jo SM**, **Seo KJ**, **Seo SS**. Long-term outcomes of high-flexion design total knee arthroplasty with a short posterior flange. *Clin Orthop Surg*. 2024;16(2):251–258.
2. **Kwon HM**, **Hong H-T**, **Kim I**, **et al**. Biomechanical effects of stem extension of tibial components for medial tibial bone defects in total knee arthroplasty: a finite element study. *J Knee Surg*. 2024;37(13):879–886.
3. **Kim KI**, **Kim JH**, **Min K**. Does the clinical and radiologic outcomes following total knee arthroplasty using a new design cobalt-chrome tibial plate or predecessor different? *Knee Surg Relat Res*. 2024;36(1):34.
4. **Song SJ**, **Lee HW**, **Kang SG**, **Bae DK**, **Park CH**. Various types of medial tibial bone resorption after total knee arthroplasty using a thick cobalt chromium tibial baseplate. *J Knee Surg*. 2022;35(4):434–442.
5. **Song SJ**, **Lee HW**, **Park CH**. Medial proximal tibial resorption after total knee arthroplasty according to the design of the cobalt chrome tibial baseplate. *Arch Orthop Trauma Surg*. 2023;143(6):3401–3407.
6. **Bendich I**, **Lawrie CM**, **Riegler V**, **Barrack RL**, **Nunley RM**. The impact of component design and fixation on stress shielding after modern total knee arthroplasty. *J Arthroplasty*. 2022;37(6S):S221–S225.
7. **Saini MK**, **Reddy CD**, **Reddy NR**, **Reddy PJ**, **Singh M**, **Bhati M**. Medial tibial bone resorption following total knee arthroplasty comparing a traditional with a kinematic design. *Arch Orthop Trauma Surg*. 2023;143(12):7139–7146.
8. **Arenas-Miquelez A**, **Barco R**, **Cabo Cabo FJ**, **Hachem AI**. Management of bone loss in anterior shoulder instability. *Bone Joint J*. 2024;106-B(10):1100–1110.

9. **Smolle MA**, **Keintzel M**, **Staats K**, **et al**. Radiolucent lines and revision risk in total knee arthroplasty using the conventional versus the Attune S+ tibial baseplate. *Bone Joint J*. 2024;106-B(11):1240–1248.
10. **Stoddart JC**, **Garner A**, **Tuncer M**, **Amis AA**, **Cobb J**, **van Arkel RJ**. Load transfer in bone after partial, multi-compartmental, and total knee arthroplasty. *Front Bioeng Biotechnol*. 2024;12:1274496.
11. **Sass J-O**, **Kebbach M**, **Lork C**, **et al**. Computational biomechanical study on hybrid implant materials for the femoral component of total knee replacements. *J Mech Behav Biomed Mater*. 2024;158:106681.
12. **Garabano G**, **Rodriguez J**, **Perez Alamino L**, **Pesciallo CA**, **Del Sel H**, **Lopreite F**. Stress shielding in total knee replacements: comparative analysis between titanium and all-polyethylene bases at 10 years follow-up. *J Orthop*. 2022;34:276–281.
13. **Wan Q**, **Han Q**, **Liu Y**, **et al**. Appropriate sagittal positioning of femoral components in total knee arthroplasty to prevent fracture and loosening. *Bone Joint Res*. 2024;13(10):611–621.
14. **Yoon C**, **Chang MJ**, **Chang CB**, **Song MK**, **Shin JH**, **Kang SB**. Medial tibial periprosthetic bone resorption and its effect on clinical outcomes after total knee arthroplasty: cobalt-chromium vs titanium implants. *J Arthroplasty*. 2018;33(9):2835–2842.
15. **Gallo J**, **Goodman SB**, **Konttinen YT**, **Wimmer MA**, **Holinka M**. Osteolysis around total knee arthroplasty: a review of pathogenetic mechanisms. *Acta Biomater*. 2013;9(9):8046–8058.
16. **Lee HH**, **Hong HT**, **Kim JK**, **Koh YG**, **Park KK**, **Kang KT**. Optimization of tibial stem geometry in total knee arthroplasty using design of experiments: a finite element analysis. *Bioengineering (Basel)*. 2025; 12(2):172.
17. **Lee JA**, **Koh YG**, **Kim PS**, **Park JH**, **Kang KT**. Effect of surface matching mismatch of focal knee articular prosthetic on tibiofemoral contact stress using finite element analysis. *Bone Joint Res*. 2023;12(8):497–503.
18. **Cho BW**, **Kang K-T**, **Kwon HM**, **et al**. Biomechanical effect of anatomical tibial component design on load distribution of medial proximal tibial bone in total knee arthroplasty: finite element analysis indicating anatomical design prevents stress-shielding. *Bone Joint Res*. 2022;11(5): 252–259.
19. **Cho BW**, **Kwon HM**, **Hong YJ**, **Park KK**, **Yang IH**, **Lee WS**. Anatomical tibial component is related to more medial tibial stress shielding after total knee arthroplasty in Korean patients. *Knee Surg Sports Traumatol Arthrosc*. 2021;29(3):710–717.
20. **Martin S**, **Saurez A**, **Ismaily S**, **Ashfaq K**, **Noble P**, **Incavo SJ**. Maximizing tibial coverage is detrimental to proper rotational alignment. *Clin Orthop Relat Res*. 2014;472(1):121–125.
21. **Kimpton CI**, **Crocombe AD**, **Bradley WN**, **Gavin Huw Owen B**. Analysis of stem tip pain in revision total knee arthroplasty. *J Arthroplasty*. 2013; 28(6):971–977.
22. **Li Y-R**, **Gao Y-H**, **Yang C**, **et al**. Finite-element analysis of the proximal tibial sclerotic bone and different alignment in total knee arthroplasty. *BMC Musculoskelet Disord*. 2019;20(1):617.
23. **Zysset PK**, **Sonny M**, **Hayes WC**. Morphology-mechanical property relations in trabecular bone of the osteoarthritic proximal tibia. *J Arthroplasty*. 1994;9(2):203–216.
24. **Kutzner I**, **Bender A**, **Dymke J**, **Duda G**, **von Roth P**, **Bergmann G**. Mediolateral force distribution at the knee joint shifts across activities and is driven by tibiofemoral alignment. *Bone Joint J*. 2017;99-B(6):779–787.
25. **Morrison JB**. The mechanics of the knee joint in relation to normal walking. *J Biomech*. 1970;3(1):51–61.
26. **No authors listed**. *Abaqus Analysis User's Manual, Version 6.11*. Providence, RI, USA: Dassault Systèmes Simulia Corp, 2011.
27. **Park HJ**, **Bae TS**, **Kang SB**, **Baek HH**, **Chang MJ**, **Chang CB**. A three-dimensional finite element analysis on the effects of implant materials and designs on periprosthetic tibial bone resorption. *PLoS One*. 2021; 16(2):e0246866.
28. **Giardullo L**, **Altomare A**, **Rotondo C**, **Corrado A**, **Cantatore FP**. Osteoblast dysfunction in non-hereditary sclerosing bone diseases. *Int J Mol Sci*. 2021;22(15):7980.
29. **Toya M**, **Kushioka J**, **Shen H**, **et al**. Sex differences of NF-κB-targeted therapy for mitigating osteoporosis associated with chronic inflammation of bone. *Bone Joint Res*. 2024;13(1):28–39.
30. **Rodríguez-Ortiz ME**, **Díaz-Tocados JM**, **Torralbo AI**, **et al**. Impact of elevated sclerostin levels on bone resorption: unravelling structural changes and mineral metabolism disruption. *Bone Joint Res*. 2025;14(5): 448–462.
31. **Naghavi SA**, **Lin C**, **Sun C**, **et al**. Stress shielding and bone resorption of press-fit polyether-ether-ketone (PEEK) hip prosthesis: a sawbone model study. *Polymers (Basel)*. 2022;14(21):4600.
32. **Linde KN**, **Rytter S**, **Langdahl BL**, **Madsen F**, **Stilling M**. Migration of cementless total knee arthroplasty is mitigated by both local intraoperative zoledronate and postoperative denosumab: a randomized controlled trial. *Bone Joint J*. 2025;107-B(8):793–803.
33. **Petis SM**, **Howard JL**, **McAuley JP**, **Somerville L**, **McCalden RW**, **MacDonald SJ**. Comparing the long-term results of two uncemented femoral stems for total hip arthroplasty. *J Arthroplasty*. 2015;30(5):781–785.
34. **Martin JR**, **Watts CD**, **Levy DL**, **Miner TM**, **Springer BD**, **Kim RH**. Tibial tray thickness significantly increases medial tibial bone resorption in cobalt-chromium total knee arthroplasty implants. *J Arthroplasty*. 2017;32(1):79–82.
35. **Zhou H**, **Chen L**, **Su H**, **Gong Y**, **Chen G**, **Tong P**. Factors influencing periprosthetic bone mineral density in total knee arthroplasty: a systematic review. *Arch Orthop Trauma Surg*. 2024;144(5):2273–2281.
36. **Lee DW**, **Ro DH**, **Han HS**, **Lee MC**. Titanium alloy knee implant is associated with higher bone density over cobalt chromium: a prospective matched-pair case-control study. *Clin Orthop Surg*. 2023; 15(4):581–588.
37. **Rivière C**, **Grappiolo G**, **Engh CA Jr**, **et al**. Long-term bone remodelling around "legendary" cementless femoral stems. *EFORT Open Rev*. 2018; 3(2):45–57.
38. **Indelli PF**, **Graceffa A**, **Marcucci M**, **Baldini A**. Rotational alignment of the tibial component in total knee arthroplasty. *Ann Transl Med*. 2016; 4(1):3.

Author information

J. Y. Park, MD, PhD, Professor,
Department of Orthopaedic Surgery, Yongin Severance Hospital, Yonsei University College of Medicine, Yongin, South Korea.

K. K. Park, MD, PhD, Professor, Department of Orthopaedic Surgery, Severance Hospital, Yonsei University College of Medicine, Seoul, South Korea.

J-H. Nam, MS, Research Engineer, Laboratory/PhD Student
K-T. Kang, PhD, CEO, Adjunct Professor
Skyve R&D LAB, Skyve Co. LTD., Seoul, South Korea; Department of Mechanical Engineering, Yonsei University, Seoul, South Korea.

M. C. Hwang, BS, Research Assistant, Skyve R&D LAB, Skyve Co. LTD., Seoul, South Korea.

B. W. Cho, MD, PhD, Assistant Professor, Department of Orthopaedic Surgery, Gangnam Severance Hospital, Yonsei University College of Medicine, Seoul, South Korea.

Author contributions

J. Y. Park: Conceptualization, Methodology, Visualization, Writing – original draft.
K. K. Park: Formal analysis, Project administration, Supervision.
J-H. Nam: Data curation, Validation.
M. C. Hwang: Resources, Software.
K-T. Kang: Software, Supervision, Writing – review & editing.
B. W. Cho: Data curation, Investigation, Writing – review & editing.

K-T. Kang and B. W. Cho contributed equally to this work.

Funding statement

The authors received no financial or material support for the research, authorship, and/or publication of this article.

ICMJE COI statement

K-T. Kang is the Chief Executive Officer of Skyve Co. Ltd., but this did not influence the results of our research. J-H. Nam and M. C. Hwang are employees of Skyve Co. Ltd., but this also did not affect the results of our research. The remaining authors declare no conflict of interest.

Data sharing

The datasets generated and analyzed in the current study are not publicly available due to data protection regulations. Access to data is limited to the researchers who have obtained permission for data processing. Further inquiries can be made to the corresponding author.

Acknowledgements

The authors used Claude (Anthropic, USA) for language editing, grammar checking, and proofreading assistance during manuscript preparation. All scientific content, research design, data collection and analysis, methodology, results interpretation, and conclusions are the original work of the authors and were not influenced by AI tools.

Ethical review statement

This study was approved by the Institutional Review Board of Yongin Severance Hospital (9-2025-0074). The requirement for informed consent was waived due to the retrospective nature of the study. The study was conducted in accordance with the Declaration of Helsinki.

Open access funding

This research received no external funding and was self-funded by the authors. OA Licence: Confirmed. CC BY-NC-ND 4.0 is correct.